

See discussions, stats, and author profiles for this publication at: <https://www.researchgate.net/publication/231706157>

On Modulating the Phase Behavior of Block Copolymer/Homopolymer Blends via Hydrogen Bonding

ARTICLE in MACROMOLECULES · DECEMBER 2009

Impact Factor: 5.8 · DOI: 10.1021/ma901729t

CITATIONS

47

READS

69

5 AUTHORS, INCLUDING:



Shih-Chien Chen

Takming University of Science and Technology

6 PUBLICATIONS 138 CITATIONS

[SEE PROFILE](#)



Shiao-Wei Kuo

National Sun Yat-sen University

267 PUBLICATIONS 5,589 CITATIONS

[SEE PROFILE](#)

On Modulating the Phase Behavior of Block Copolymer/Homopolymer Blends via Hydrogen Bonding

Shih-Chien Chen,[†] Shiao-Wei Kuo,^{*,‡} U-Ser Jeng,[§] Chun-Jen Su,[§] and Feng-Chih Chang^{*,†}

[†]Institute of Applied Chemistry, National Chiao Tung University, Hsin Chu, 300 Taiwan, [‡]Department of Materials and Optoelectronic Science, Center for Nanoscience and Nanotechnology, National Sun Yat-Sen University, Kaohsiung, 804 Taiwan, and [§]National Synchrotron Radiation Research Center, Hsin Chu Science Park, Taiwan

Received August 3, 2009; Revised Manuscript Received December 4, 2009

ABSTRACT: We have investigated the phase behavior of poly(4-vinylphenol-*b*-styrene) (PVPh-*b*-PS) when respectively blended with poly(4-vinylpyridine) (P4VP), poly(methyl methacrylate) (PMMA), and PVPh homopolymers by mediated hydrogen bonding strengths with the PVPh block of the copolymer. The Fourier transform infrared spectroscopic result indicates that the PVPh-*b*-PS/P4VP blend has a much higher fraction (f_H) of hydrogen-bonded PVPh blocks for a significantly higher miscibility compared with the blends with PMMA and PVPh homopolymers. Consequently, the PVPh-*b*-PS/P4VP blend, behaving as a neat diblock copolymer, exhibited a series of order–order phase transitions from the lamellar, gyroid, hexagonally packed cylinder to body-centered cubic structures when the P4VP content increases from 6 to 71% (volume fraction), as evidenced consistently by transmission electron microscopy and small-angle X-ray scattering. In contrast, both the PVPh-*b*-PS/PMMA and PVPh-*b*-PS/PVPh blends maintained essentially the lamellar structure upon a similar volume fraction increase in the homopolymers; the lamellar structure, however, was distorted to different extents at higher volume fractions of the additives, depending on the hydrogen bonding strength. On the basis of the results, the ratio of interassociation equilibrium constant (K_A) over self-association equilibrium constant (K_B), K_A/K_B , is introduced as a convenient guide in estimating the phase behavior of similar polymer blends featuring hydrogen bonding interactions between the homopolymer additive and copolymer: with a K_A/K_B ratio much larger than unity, the blend system tends to behave as a neat copolymer; with a K_A/K_B ratio significantly smaller than unity, phase separation instead of order–order phase transitions can be expected for the blend above certain volume fraction of homopolymer additive.

Introduction

Self-assembly of block copolymers plays a key role in the design of new functional supramolecular materials for a wide range of applications such as pollution control and drug delivery.^{1,2} Blending homopolymers into diblock copolymers for enriched phase behaviors furthermore broadens the applications.^{3–28} An efficient blend of such kind, however, critically depends on (1) the ratio of the molar weight of the additive homopolymer to that of the associated block of the copolymer and (2) the volume fraction and miscibility of the additive homopolymer in the blend.^{29–40}

In blends based on a diblock copolymer (A-*b*-B) and a homopolymer (C), where C is different from A and B, the phase behavior is particularly rich because of more parameters available on controlling the miscibility between the homopolymer and the two blocks of the copolymer, as demonstrated by a significant number of studies.^{39–44} Depending on the miscibility between C/A and C/B and A/B, there can be several interesting combinations for the blending; here we are interested in one of them where A and B are immiscible and C is miscible with B but immiscible with A. Along this line of study, Ikkala et al. prepared blends from a polyisoprene-*b*-poly(2-vinyl pyridine) (PI-*b*-P2VP) copolymer added with a novolac resin that is immiscible with the PI block.⁴⁵ Dobrosielska et al. studied various microphase-separated structures of the poly(vinyl phenol) (PVPh)/poly(styrene-*b*-2-vinylpyridine) (PS-*b*-P2VP) blend system, in which PVPh and

P2VP are miscible through strong hydrogen bonding but PVPh and PS are immiscible.^{46,47} Zhao et al. investigated blends of poly(styrene-*b*-vinyl phenol) (PS-*b*-PVPh) diblock copolymers with several homopolymers having hydrogen bonding acceptors, such as poly(ethylene oxide) (PEO), poly(4-vinyl pyridine) (P4VP), and poly(butyl methacrylate) (PBMA); these homopolymers are immiscible with the PS block.⁴⁸ In all of these studies mentioned, hydrogen bonding plays a critical role in modulating the miscibility between the additives and the copolymers, resulting in enriched morphology transitions for the polymer blends.

Inspired by the studies mentioned, we intend to quantify the influence of hydrogen bonding on the phase behavior of homopolymer-copolymer blends of the A-*b*-B/C type, basing on a model system of PVPh-*b*-PS diblock copolymer respectively blended with homopolymers of different hydrogen bonding strengths (therefore different miscibilities) with the PVPh blocks, including poly(4-vinylpyridine) (P4VP), poly(methyl methacrylate) (PMMA), and PVPh. The three additives are immiscible with the PS blocks. With Fourier transform infrared (FTIR) spectroscopy, we map out the fraction of hydrogen bonded groups as a function of the additive volume fraction for the polymer blends, where the molar weight of the additive homopolymer should be comparable to or smaller than the corresponding block; the corresponding thermal properties and phase behavior, including microphase-separated structures and order–order phase transitions, are elucidated by differential scanning calorimetry (DSC), transmission electron microscopy (TEM), and small-angle X-ray scattering (SAXS). Integrating these results, we correlate quantitatively the hydrogen bonding strength with the phase behavior of the polymer blends.

*To whom correspondence should be addressed. E-mail: changfc@mail.nctu.edu.tw. Tel: 886-3-5131512. Fax: 886-3-5131512 (F.-C.C.); E-mail: kuosw@faculty.nsysu.edu.tw. Fax: 886-7-5254099 (S.-W.K.).

Table 1. Molecular Weights of PVPh-*b*-PS, PVPh, PMMA, and P4VP Used in Preparing the Polymer Blends^a

polymer	M_n	M_w/M_n
PVPh ₆₃ - <i>b</i> -PS ₁₀₉ (HS)	18 900	1.07
PVPh ₄₂ (H)	5040	1.05
PMMA ₅₃ (M)	5300	1.18
P4VP ₅₂ (V)	5460	1.12

^a Volume fractions of PVPh and PS blocks in the neat block copolymer are, respectively, 37.6 and 62.4%.

Experimental Section

Block Copolymer and Homopolymer Syntheses. The PVPh-*b*-PS diblock copolymer and the PVPh, P4VP, and PMMA homopolymers were synthesized through sequential anionic polymerization, as described in the Supporting Information; their molecular weights are summarized in Table 1.^{49–53}

Sample Preparation. Blends of PVPh-*b*-PS/P4VP, PVPh-*b*-PS/PMMA, and PVPh-*b*-PS/PVPh (denoted as HS/V, HS/M, and HS/H, respectively) with a series of volume fractions of homopolymer up to 70% were prepared through solution casting. After stirring for 6–8 h, thin films specimens were cast on Teflon dishes from dimethylformamide (DMF) solutions containing 5 wt % polymer mixture, followed by a slow evaporation at 100 °C for 7 days and a subsequent thermal annealing at 120 °C under vacuum for another 7 days. Samples thus prepared could be reproduced for the same thermal properties and same structures.

Characterization Methodology. DSC traces were measured using a DuPont TA Instrument Q-20 controller at a scan rate of 20 °C/min over the temperature range from 30 to 250 °C under N₂. Infrared spectra were recorded with a resolution of 1 cm^{−1} using a Nicolet Avatar 320 FTIR spectrometer under N₂; the vacuum-dried sample thin films, satisfying the Beer–Lambert law within the absorbance range, were cast directly onto KBr pellets from the DMF sample solutions.

TEM images were taken for the samples with either the PS block stained with RuO₄ or the P4VP block with I₂, using a Hitachi H-7500 transmission electron microscope operated at an accelerating voltage of 100 kV. Ultrathin sections of the TEM samples (ca. 70 nm thickness) were prepared using a Leica Ultracut UCT micromtome equipped with a diamond knife. SAXS experiments were performed using the BL23A SWAXS instrument at the National Synchrotron Radiation Research Center (NSRRC), Taiwan,^{43,44,54,55} using a 10 keV (wavelength $\lambda = 1.24 \text{ \AA}$) beam with a 0.5 mm diameter. The scattering wave-vector transfer $q = 4\pi\lambda^{-1} \sin \theta$ is defined by λ and the scattering angle 2θ of X-rays. Samples for SAXS (thickness ~1 mm) were sealed between two thin Kapton windows (80 μm thickness each) and measured at an ambient temperature ~26 °C.

IR Data Analysis. The fractions of hydrogen-bonded pyridine rings of the PVPh block in the polymer blends were estimated using⁵⁶

$$f_b = \frac{A_b/a}{A_b/a + A_f} \quad (1)$$

where A_f and A_b are integrated areas over two characteristic absorption bands of the free and the hydrogen-bonded functional groups; the conversion coefficient a is the specific absorption ratio between the two absorption bands. For the HS/M system, absorptions of the free and hydrogen-bonded C=O groups of PMMA at 1730 and 1705 cm^{−1}, respectively, were selected to calculate A_f and A_b and therefore f_b values, with $a = 1.5$ suggested by Moskala et al.⁴ For the HS/V blends, f_b values were calculated on the basis of the two characteristic absorptions bands at 993 and 1005 cm^{−1} related to the free and hydrogen-bonded pyridine rings of P4VP, together with $a = 1$ suggested by Moskala et al. (cf. Supporting Information).⁵⁷

SAXS Data Analysis. SAXS data with lamellar peaks were analyzed using the 1D correlation function

$$\gamma(x) = \frac{1}{Q} \int_0^\infty I(q) q^2 \cos(qx) dq \quad (2)$$

obtained from the Fourier transform of the corresponding 1D SAXS intensity profile $I(q)$ with the scattering invariant $Q = \int_0^\infty I(q) q^2 dq$.⁵⁸ For an ideal two-phase lamellar structure, the first maximum of $\gamma(x)$ corresponds to the long period D of the lamellae; the thickness of the thinner phase l_c of the lamellar stacks can be estimated from the intersection of the two lines passing, respectively, the first minimum and the first inflection point of the correlation function, as illustrated in the Supporting Information (Figure S3-d). Because the $\gamma(x)$ function cannot account for the interfacial zone width, D_{tr} , of the studied blends of a nonideal two-phase structure, the layer thicknesses for the PS-block layer and the PVPh-homopolymer layer thus extracted are smeared over the interfacial zone thickness.

To extract D_{tr} for the blends with a lamellar morphology, direct Fourier transform with phase factors taken into account was applied to the SAXS data for a relative electron density profile⁵⁹

$$\rho_e(z) \approx \sum_{k=1}^n \sqrt{I(q_k) q_k^2} \varphi_k \cos(q_k z) \quad (3)$$

Here n is the total number of diffraction orders observed ($n > 3$ for a more reliable electron density profile), and q_k , $I(q_k)$, and φ_k are, respectively, the scattering vector, integrated intensity, and phase factor of the k^{th} reflection. For a centrosymmetrical system, φ_k is either +1 or −1. It was found that for the polymer blend studied, the most reasonable combination for the phase factors of the first four lamellar peaks is (−1, +1, +1, −1); with the phase factors, the extracted electron densities for the mixed PVPh–P4VP, PVPh–PMMA, and PVPh–PVPh layers are, as expected, higher than that of the PS layer.

Results and Discussion

FTIR Result. As shown in Figure 1a,b are the two IR spectra for the HS/V and HS/M blends. Figure 1c displays the corresponding f_b profiles deduced from the IR spectra mainly based on the two chrematistic absorptions at 993 and 1005 cm^{−1} for the HS/V blends and 1730 and 1705 cm^{−1} for the HS/M blends, as previously detailed. The f_b values for the HS/V system are systematically much higher than that of the HS/M system, reflecting a substantially better hydrogen bonding efficiency. This result is consistent with the much higher K_A/K_B value (~16) (for the ratio between inter- and self-association equilibrium constants derived based on the PCAM model⁵⁵) of the HS/V blend system than that ($K_A/K_B \approx 0.6$) for the HS/M blend. IR spectra taken for the two systems in the range 2700–4000 cm^{−1} consistently reveal a much stronger hydrogen bonding strength for the HS/V system, as detailed in the Supporting Information. The deduced f_b values (and their multiplies with the volume fractions for hydrogen-bonded volume fractions) serve as a guide for the order–order morphology transitions of the polymer blends, as detailed below.

Thermal Properties. Figure 2 presents the DSC traces of PVPh-*b*-PS, PVPh, PMMA, P4VP, and the blends with systematically increased volume fractions of the homopolymers. The pure PS-*b*-PVPh diblock copolymer exhibits two glass transitions at 108 and 167 °C, corresponding to the PS and PVPh phases, respectively. The increases in both T_g values of the PS and PVPh blocks (relative to the homopolymers) are attributed to the microphase separation effect

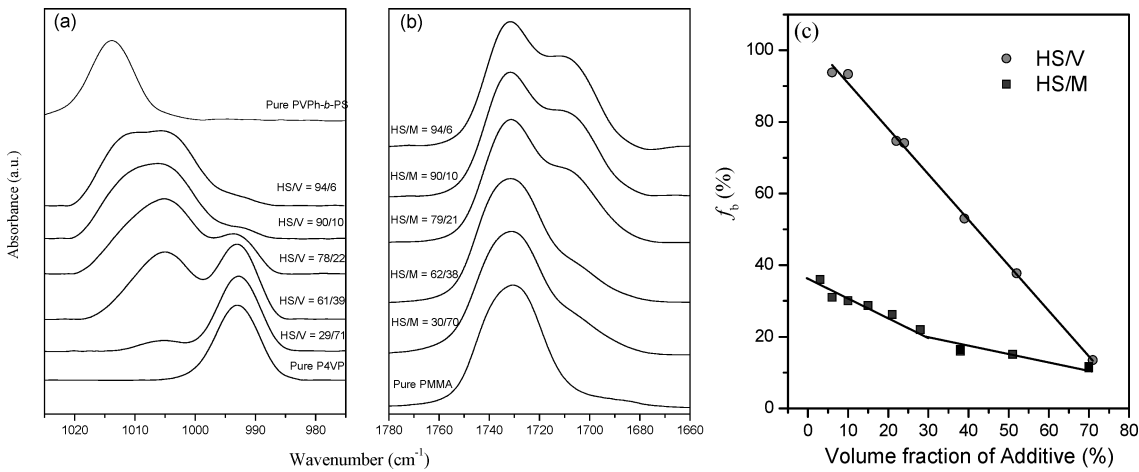


Figure 1. FTIR spectra recorded at 120 °C in (a) the pyridine absorption region for the HS/V blends and (b) the C=O absorption region for the HS/M blends. The compositions are indicated above the respective profiles. (c) The corresponding f_b values for the fraction of hydrogen-bonded groups. Lines drawn over the data points are only for eye-guiding. The decrease in f_b (i.e., reduction of hydrogen bonding efficiency) with the increase in the homopolymer volume fraction reveals a systematically decreased miscibility in both blends.

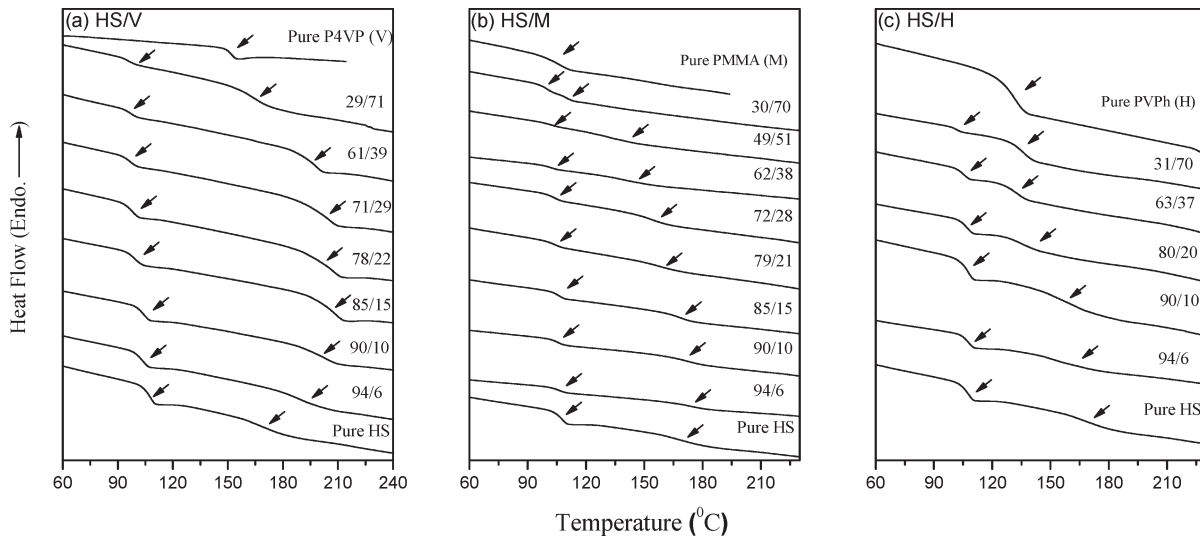


Figure 2. DSC traces of the (a) HS/V, (b) HS/M, and (c) HS/H blends, with the respective compositions indicated. Arrows indicate the respective T_g values.

of the block copolymer and the much higher molecular weight of the PVPh block (approximately four-fold) than the homopolymer, as revealed by FTIR and X-ray diffraction (cf. the Supporting Information, Figure S4). For homopolymers, T_g values of 152, 105, and 133 °C were observed for P4VP, PMMA, and PVPh, respectively. For all HS/V blends, two distinct T_g values could be observed, corresponding to the PS phase and the mixed phase of PVPh-P4VP, respectively; this result indicates that the blend can form a stable mixed phase with a wide range of homopolymer volume fraction, which is essential for order-order phase transitions (detailed below). In contrast, the T_g for the mixed phase of PVPh-PMMA is, in general, less clear-cut and decreased systematically in value upon an increase in the PMMA content, implying a less-stable mix phase with respect to the addition of homopolymer, presumably, owing to a smaller hydrogen bonding strength. The even faster drop in the T_g value of the mixed phase of the HS/H blend upon increasing the content of the PVPh homopolymer up to 20 vol % because low-molecular-weight homopolymer added must be responsible for the T_g decrease in the PVPh phase. Upon further addition of PVPh homopolymer, T_g of the

mixed phase was replaced by T_g of the PVPh homopolymer; this implies a solubility limit of ~20% of PVPh homopolymer in the PVPh blocks of the copolymer.

Order-Order Structural Transitions for the HS/V Blends. The TEM images shown in Figure 3 for the HS/V blends exhibited a series of order-order phase transitions from the lamellar, gyroid, hexagonally packed cylinder (HCP), to body-centered cubic (BCC) structures as the volume fraction of P4VP increases from 6 to 13, 15–22, 29, to 71%. Such phase transition behavior of the blend closely follows that for a neat diblock copolymer, implying a collective behavior of PVPh and P4VP chains in the mixed phase.

Complementarily, SAXS profiles for the HS/V system in Figure 4 display scattering patterns that match nearly ideally to the structures observed by TEM (Figure 3). Specifically, the SAXS profiles for the neat diblock copolymer PVPh-*b*-PS and HS/V blends with compositions of 94/6, 90/10, and 87/13, all demonstrate lamellar peaks that are consistent with the TEM images in Figure 3a–d. Similar SAXS profiles were observed for the blends with compositions 85/15, HS/V = 78/22, and HS/V = 76/24; the first four scattering peaks can be associated with the (211), (220), (321), and (332) reflection

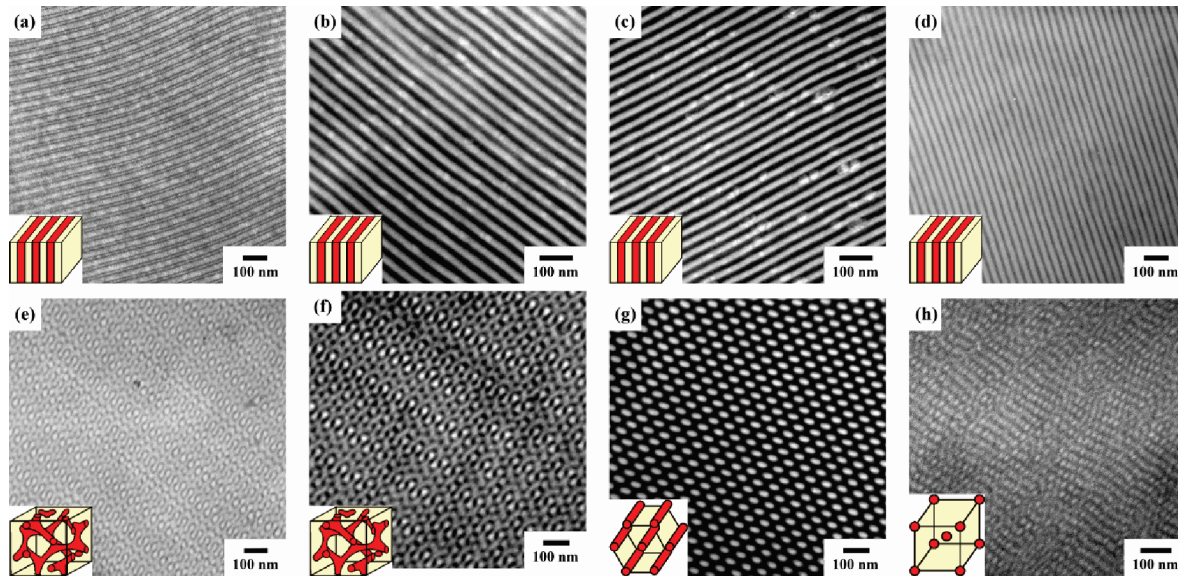


Figure 3. TEM images for the HS/V blends after staining with I_2 for 24 h (the dark regions correspond to the PVPh–P4VP phase): (a) pure HS and HS/V = (b) 94/6, (c) 90/10, (d) 87/13, (e) 85/15, (f) 78/22, (g) 71/29, and (h) 29/71. Shown in the insets are the corresponding structures proposed.

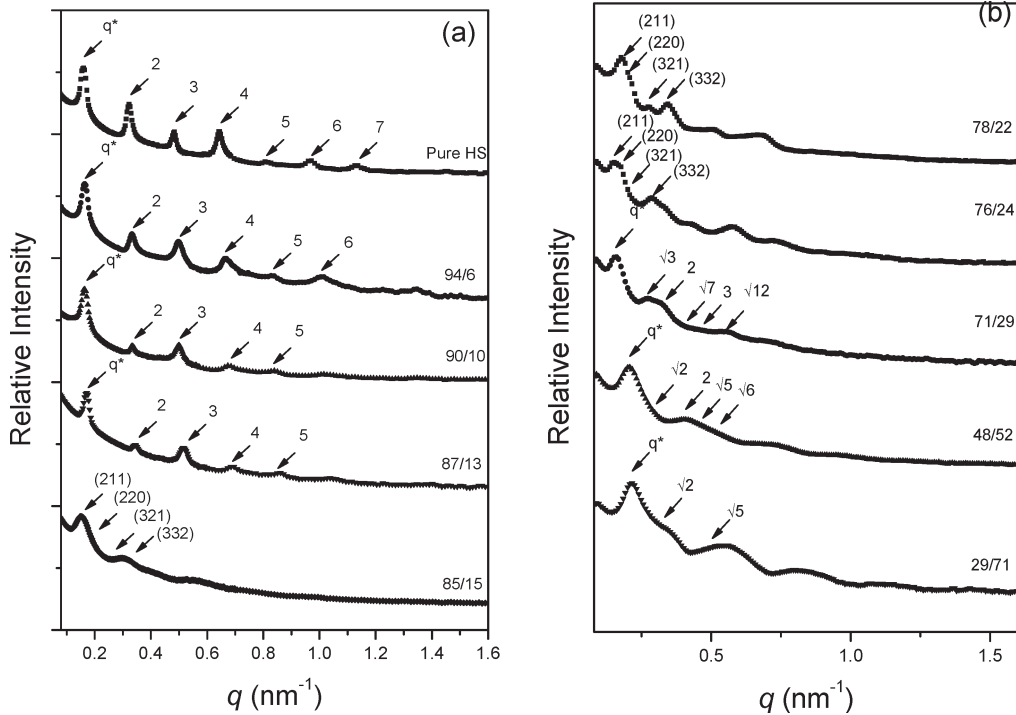


Figure 4. SAXS data for (a) the pure HS and the blends HS/V = 94/6, 90/10, 87/13, and 85/15 and (b) the blends HS/V = 78/22, 76/24, 71/29, 48/52, and 29/71. The peak ratios (relative to the first peak position marked as q^*) or reflections planes for the corresponding ordered structures are indicated by arrows.

planes, of a gyroid structure, which has been evidenced by the TEM images shown in Figure 3e–f. With the P4VP content increased to 29%, the SAXS profile clearly exhibits organized peaks with peak ratios $1:\sqrt{3}:2:\sqrt{7}:3:\sqrt{12}$, indicating hexagonally packed cylinders, as also imaged in Figure 3g. With further increased P4VP contents to 52 and 71%, the corresponding SAXS profiles both show scattering peaks with ratios of $1:\sqrt{2}:\sqrt{5}$, indicating microseparated domains with BCC-packed spheres, as visualized in Figure 3h.

Order–Disorder Structural Transitions for the HS/M and HS/H Blends. The HS/M and HS/H blending systems show, respectively, modest and low hydrogen bonding between

homopolymer and copolymer, as compared with the HS/V blends. Consequently, TEM images (Figure 5 and 6) taken for the two systems mainly show the order-to-disorder (lamellar to distorted lamellar) structural change when the volume fraction of the additive increased in the same range (6–70%) as that in HS/V system. At high volume fractions of additives, phase separation of the additive homopolymers was observed, in particular, in the HS/H blends with weak hydrogen bonding. Before phase separation, an intermediate structure of swollen lamellae coexisting with the unswollen ones could be observed (Figure 5e and 6c,d) for both systems, as also evidenced from the broad double peaks in the corresponding SAXS profiles (indicated by the thick arrows

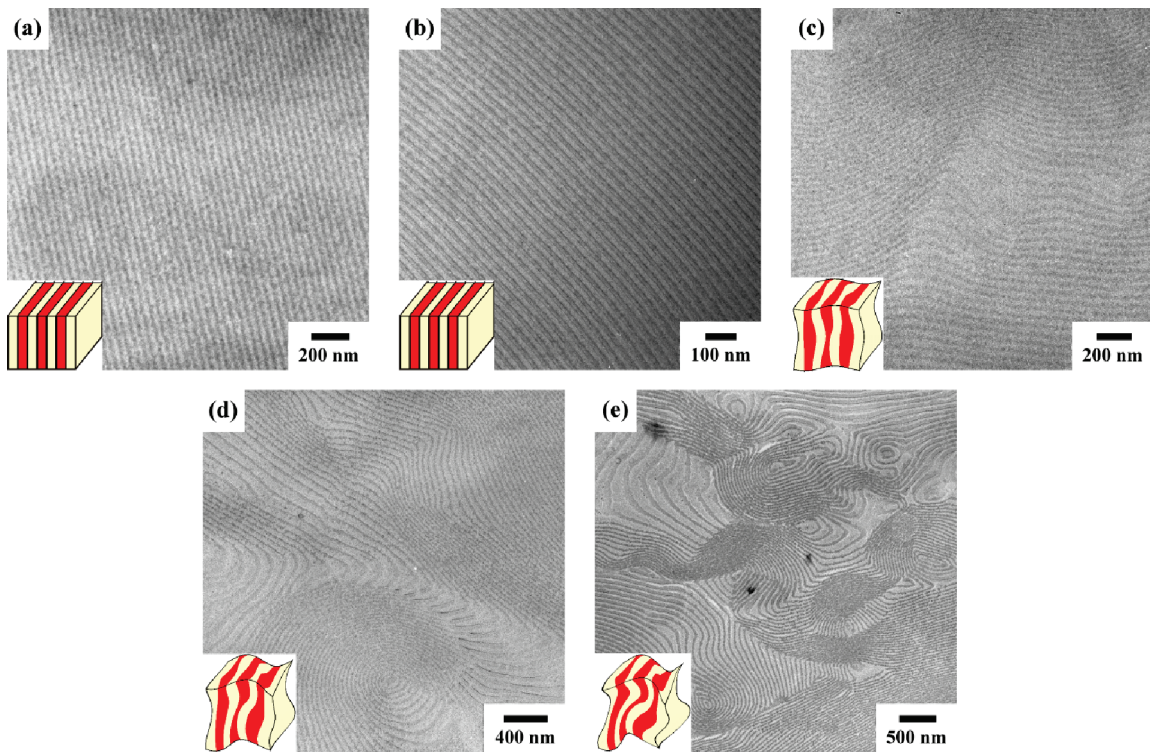


Figure 5. TEM images of the solution-cast films of the HS/M blends (dark regions correspond to the PS domains): HS/M = (a) 94/6, (b) 90/10, (c) 79/21, (d) 62/38, and (e) 30/70. Cartoons in the insets present the corresponding structures proposed.

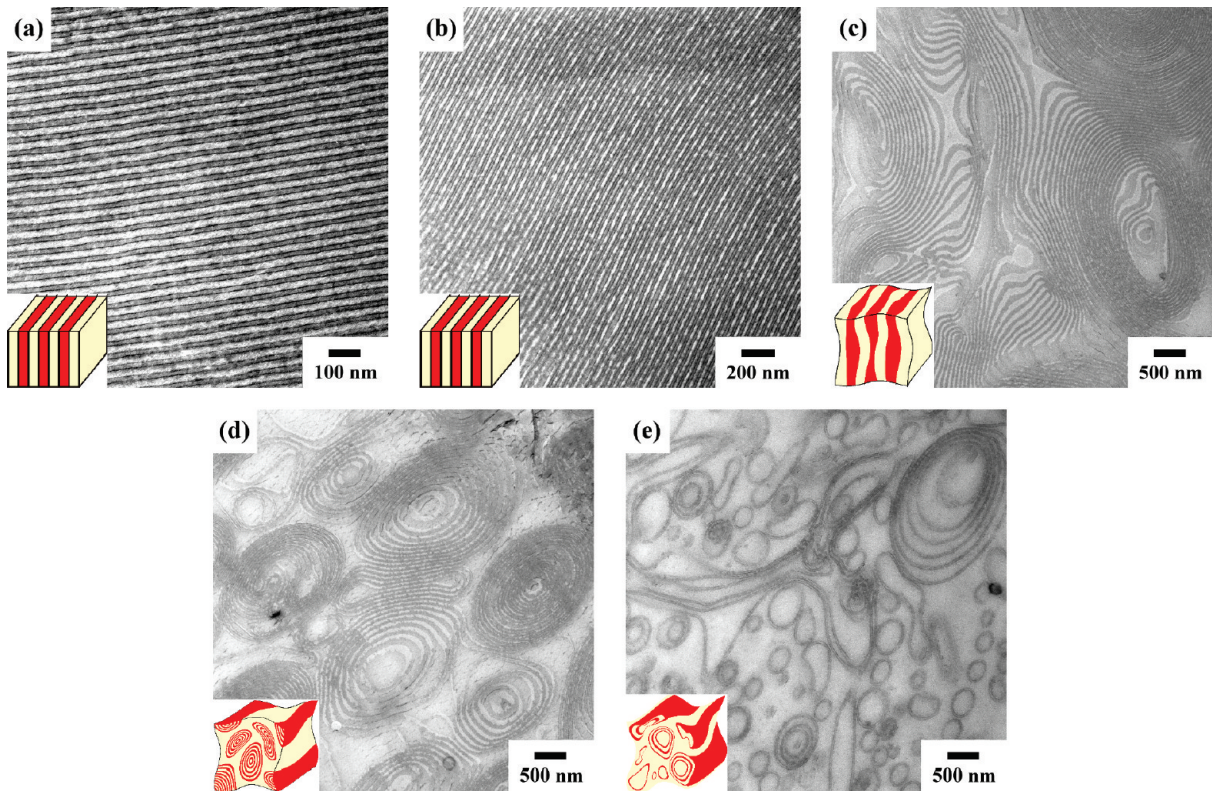


Figure 6. TEM images of the solution-cast films of the blends (dark regions correspond to the PS domains): HS/H = (a) 94/6, (b) 90/10, (c) 80/20, (d) 63/37, and (e) 31/69. Proposed 3-D structures are shown in the insets. (d,e) Concentric tubes and hollow tubes (of a single-bilayer wall) rolled from the distorted lamellar slabs.

in Figure 7a,b). In particular, for the HS/H blends, the TEM image (Figure 6e) indicates that the large amount of homopolymer finally discretizes the lamellae of the diblock copolymer into single slabs (single bilayers); previously, the DSC

result has also suggested a dissociation of the mixed phase based on the diminishing T_g (Figure 2c). Likely, upon loosing the steric interactions between the lamellar slabs, the dangling slabs bent and curve in the excess homopolymer

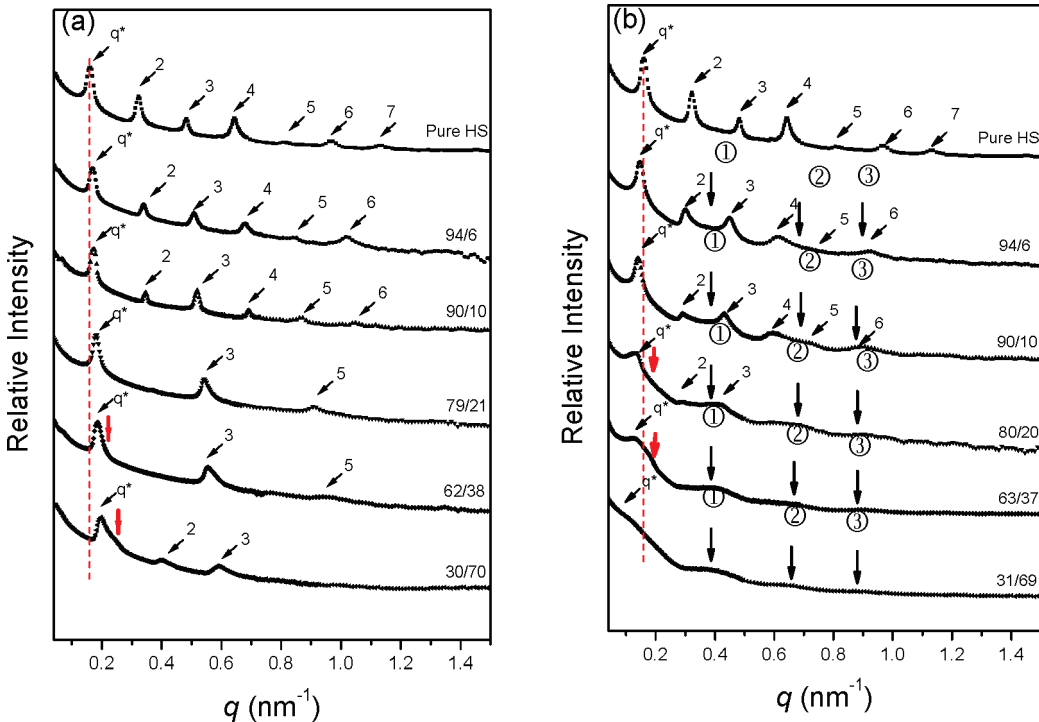


Figure 7. SAXS intensity profiles measured for the (a) HS/M and (b) HS/H blends, with the respective compositions indicated. The lamellar reflections are marked by the thin arrows, whereas the scattering humps from the form factor of slabs are marked with circled numbers in part b. The thick arrows nearby the first lamellar peaks indicate the coexisting of two types of lamellae. In parts a and b, the two dotted lines across all SAXS profiles for the HS/V and HS/M blends illustrate the opposite shifting directions of the first peak position.

phase; the formation of hollow tubes with a single-bilayer wall, as shown in Figure 6e, however, is a surprising.

Shown in Figure 7a,b is a series of SAXS profiles for the HS/M and HS/H systems. Unlike that for the order–order phase transition in the HS/V system, these SAXS profiles essentially reflect that the lamellar structure in either system is gradually distorted upon the increase in homopolymer, as that shown in the corresponding TEM images (Figures 5 and 6). Up to 70 vol % of the additive, the three residual lamellar peaks in the SAXS profile (Figure 7a) indicate that the HS/M system of weak hydrogen bonding strength can essentially hold the lamellar structure. Whereas in the HS/H system, the first lamellar peak melts in the SAXS profile (Figure 7b) at this high volume fraction of additive (70%), implying that the lamellar structure is completely destroyed; this is consistently observed in the DSC and TEM results previously shown. Note that the three broad scattering maxima in the SAXS profile (indicated by the thick arrows marked with circled numbers in Figure 7b) are not the lamellar peaks; rather, they are contributed by the form factor scattering of isolated PS layers (cf. the TEM image in Figure 6e), as calculated using a slab geometry with a slab thickness of 24 nm.

To illustrate the reliability of the prescribed volume fractions for the mixed phase in these blends, we note that in the SAXS profile of the neat HS containing ~40 vol % PVPh, the fifth reflection (Figure 7a) nearly diminishes as it should be, owing to a destructive interference under this volume fraction; upon the addition of 21% PMMA to the blend for equal volume fractions of the PS and PVPh-PMMA phases (i.e., the 79:21 case in Figure 7a), lamellar peaks of even orders of destructive phase factors disappear accordingly. Interestingly, the two sets of SAXS profiles of the HS/M and HS/H blends illustrate opposite shifting of the first peak position; namely, the first peak in the HS/M blend shifts systematically toward higher- q region as the PMMA content

increases, corresponding a shrinkage of the lamellar spacing. In the case of HS/H blends, the first lamellar peak shifts toward lower q upon increasing the PVPh content, corresponding to an increase in the lamellar spacing. The origin of this dissimilarity is discussed below on the basis of the hydrogen bonding (attractive interactions) of the additive homopolymers with the copolymer.

Correlation between the Hydrogen Strength and Phase Transition. The DSC, TEM, and SAXS results collectively show that the HS/V blends follow a phase transition behavior similar to that of a neat copolymer of PS-*b*-PVPh. The HS/M and HS/H blends are subject to phase separation to different extents at high volume fractions of homopolymer additives. Integrating the FTIR result in Figure 1c, we further correlate the hydrogen bonding strength to the phase behaviors of the polymer blends. We show in Figure 8 that the lamellar-to-gyroid phase transition in similar polymer blends may require a fraction of hydrogen-bonded groups in the range of $0.3 \lesssim f_b \lesssim 0.8$ at a mixed phase volume fraction $V_{\text{mix}} \approx 46\%$; transition from gyroid to HCP may occur with $0.20 \lesssim f_b \lesssim 0.65$ at $V_{\text{mix}} \approx 56\%$, whereas $0.15 \lesssim f_b \lesssim 0.38$ at $V_{\text{mix}} \approx 70\%$ for HCP-to-BCC transition.

Figure 8 provides a quantitative correlation between the phase behavior and the hydrogen bonding strength (efficiency) for the PS-*b*-PVPh-based, A-*b*-B/C type of polymer blends. Furthermore, on the basis of the Painter–Coleman association model (PCAM) and the interassociation equilibrium constant K_A and self-association equilibrium constants K_B , we suggest the simple ratio K_A/K_B can also be used as a convenient guide in estimating the phase behavior of similar polymer blends. The K_A and K_B values for the hydrogen-bonded PVPh/P4VP ($K_A = 598$) and PVPh/PMMA ($K_A = 37.4$) and the self-association equilibrium constant for PVPh ($K_B = 66.8$) have been determined previously.^{50,56,60} On the basis of these values, the phase behavior of the HS/V blends with $K_A/K_B \approx 9$ ($\gg 1$) of strong

hydrogen bonding strength closely follows that of a typical diblock copolymer; with $K_A/K_B \approx 0.6$ for the HS/M blends, phase separation instead of order–order transition is observed above certain volume fraction of homopolymer, as illustrated in Figure 9.

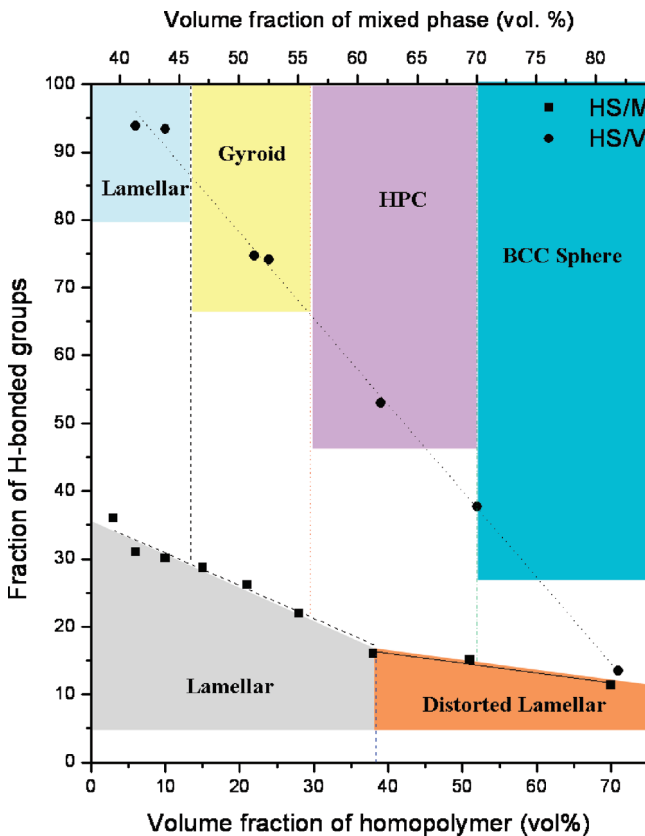


Figure 8. Correlation between the fraction of hydrogen bonded groups, f_b , deduced from FTIR and the phase behavior observed via TEM and SAXS for the PS-*b*-PVPh-based A-*b*-B/C type of polymer blends.

Distribution/Chain Conformation of the Additive Homopolymers in the Blends. As we have clarified, the hydrogen bonding effect on the phase behavior of the A-*b*-B/C type of polymer blends based on PS-*b*-PVPh, with P4VP, PMMA, and PVPh additives, we are now in a good position to examine how additive homopolymers conform and distribute their chains in the blends to fulfill the different structural characteristics required for the different ordered phases observed.

Summarized in Table 2 are the thicknesses of the PS layer, D_{PS} , the mixed layer (of PVPh-homopolymer), D_{mix} , and the long period, D , of all of the blends of lamellar morphology, obtained from the 1-D correlation function (cf. Figure S3 in Supporting Information); the relative changes in D upon the addition of homopolymers, that is, D/D_0 , where $D_0 = 39$ nm is the D value for the neat copolymer, are presented in Figure 10a. Furthermore, the correlated changes in the average distance, a_J , of the chemical junctions along the interface and thus the relative changes a_J/a_{J0} (where a_{J0} is for the neat copolymer) can be derived for the blends. Simple volumetric conservation leads to $D/D_0 = (\rho_J/\rho_{J0})\Phi_{block}^{-1}$ for a lamellar structure, where ρ_J is the number of block chains per unit interfacial area ($\sim a_J^2$) and thus $a_J/a_{J0} \approx (\rho_J/\rho_{J0})^{-1/2}$,^{3,61} and Φ is the volume fraction of the block copolymer in the blend. Similarly, $D/D_0 = (\rho_J/\rho_{J0})[(2/\sqrt{3})\pi f\Phi_{block}^{-1}]^{1/2}$

Table 2. Thicknesses of the PS (D_{PS}) and PVPh-Homopolymer Layers (D_{mix}) Determined from 1-D Correlation Function

sample	D_{PS} (nm)	D_{Mix} (nm)	D (nm)
HS	23.6	15.4	39.0
HS/H = 94/6	23.7	18.2	41.9
HS/H = 90/10	24.1	19.8	43.9
HS/H = 80/20	25.9	21.4	47.3
HS/M = 94/6	21.4	15.6	37.0
HS/M = 90/10	20.3	16.1	36.4
HS/M = 79/21	18.9	15.6	34.5
HS/M = 62/38	18.3	15.1	33.4
HS/M = 31/69	18.1	13.1	30.2
HS/V = 94/6	21.2	16.5	37.7
HS/V = 90/10	20.7	17.2	37.9
HS/V = 87/13	19.3	17.0	36.3

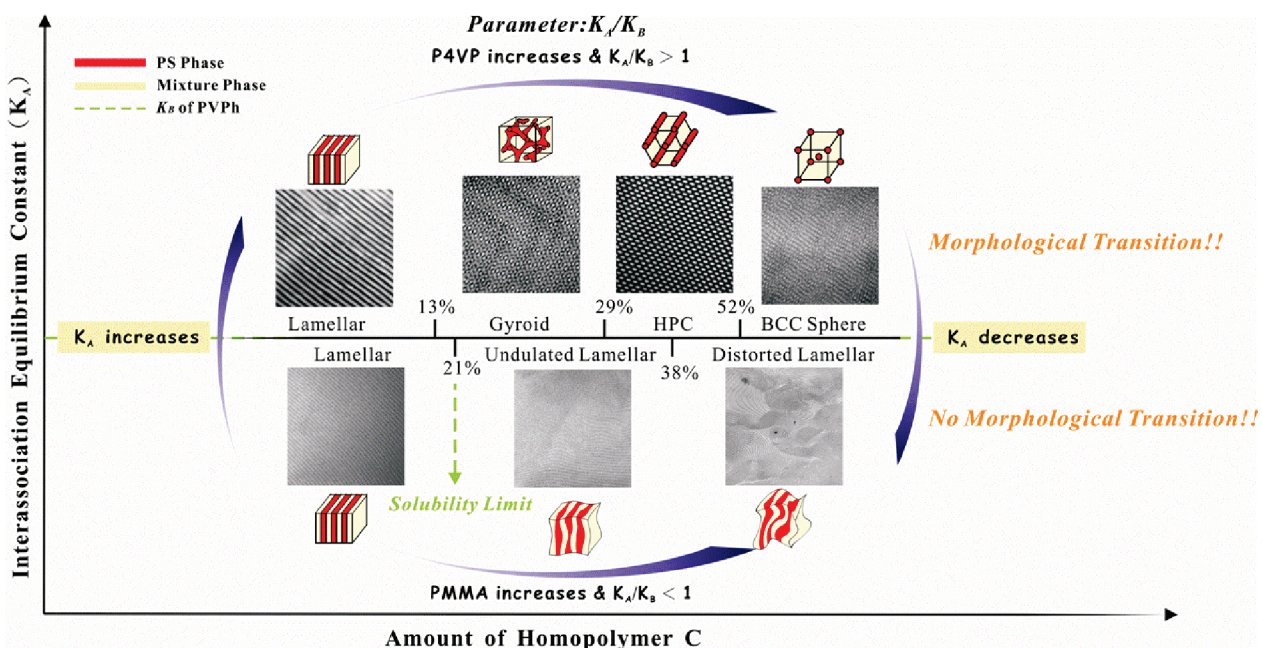


Figure 9. Schematic representation of an A-*b*-B/C blend system featuring hydrogen bonding interactions. Note that the molar weight of the homopolymer should be comparable to or smaller than that of the hydrogen-bonding-associated block of the copolymer.

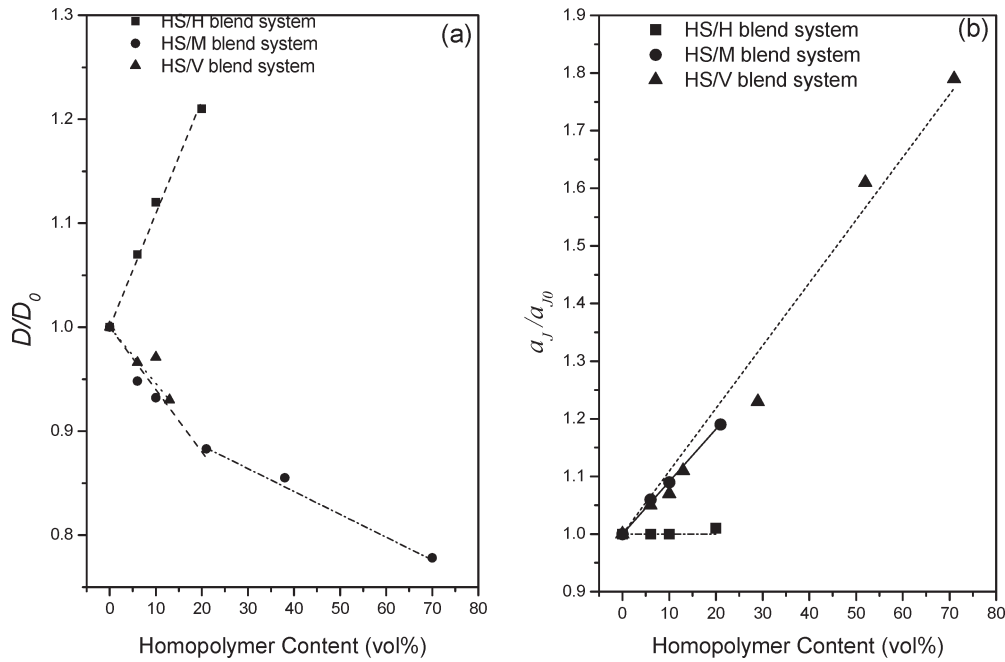


Figure 10. Relative changes in (a) the lamellar long period D/D_0 and (b) the average distance of the chemical junctions along the interface a_j/a_{j0} for the HS/H, HS/M, and HS/V blends upon the addition of the homopolymer. The lines over the data points are only for eye-guiding.

Table 3. Relative Changes (with Respective to the Neat Copolymer) in D , ρ_j , and a_j for the HS/H, HS/M, and HS/V Blends^a

sample	morphology	D/D_0	ρ_{j0}/ρ_j	a_j/a_{j0}
HS	lamellar	1	1	1
HS/H = 94/6	lamellar	1.07	1.01	1
HS/H = 90/10	lamellar	1.12	1.01	1
HS/H = 80/20	lamellar	1.21	0.97	1.01
HS/M = 94/6	lamellar	0.95	0.89	1.06
HS/M = 90/10	lamellar	0.93	0.84	1.09
HS/M = 79/21	lamellar	0.88	0.71	1.19
HS/M = 62/38	lamellar	0.86		
HS/M = 30/70	lamellar	0.78		
HS/V = 94/6	lamellar	0.97	0.9	1.05
HS/V = 90/10	lamellar	0.97	0.87	1.07
HS/V = 87/13	lamellar	0.93	0.81	1.11
HS/V = 85/15	gyroid			
HS/V = 78/22	gyroid			
HS/V = 76/24	gyroid			
HS/V = 71/29	hp cylinder	0.66	1.23	
HS/V = 48/52	bcc sphere	0.39	1.6	
HS/V = 29/71	bcc sphere	0.31	1.8	

^a Interdomian spacing for the HS/V blends 71/29 (HPC), 48/52 (BCC spheres), and 29/71 (BCC spheres) are 45.6, 37.4, and 35.7 nm, respectively.

for hexagonally packed cylinders and $D/D_0 = (\rho_j/\rho_{j0}) \cdot [(27\sqrt{3}/8)\pi/\Phi_{block}^{-1}]^{1/2}$ for BCC spheres, as suggested by Hashimoto et al.³ On the basis of these relations, we have derived the values of ρ_j/ρ_{j0} and a_j/a_{j0} for the blends, which are summarized in Table 3 and Figure 10b.

For the HS/H blends with low volume fractions of the additive homopolymer (<20%), Figure 10a exhibits a nearly linear growth of D/D_0 with the homopolymer volume fraction, accompanied by a constant a_j/a_{j0} (= 1) (Figure 9b). Such a result suggests that the homopolymer additive prefers to stay in between the PVPh blocks and does not intervene in the interface of the PS and PVPh blocks. With such a behavior, continuous swelling of the mixed phase with higher and higher volume fractions of PVPh homopolymer inevitably discretizes the lamellae of the diblock copolymer into single bilayers, as evidenced in the TEM and SAXS results.

In contrast, both the HS/M and HS/V blends characterized with hydrogen bonding display a contraction in the lamellar spacing, that is, $D/D_0 < 1$ (Figure 10a) accompanied by an expansion in a_j , ($a_j/a_{j0} > 1$ in Figure 10b). Presumably, the additive homopolymers can intervene in (and wet) the PVPh chains of the block copolymer at the interfaces, resulting in the observed expansion in a_j . The PS blocks, being chemically linked to the PVPh blocks, cannot but contract to accommodate the expanded interface zone. Consequently, the PS layer thickness and thus the lamellar spacing, decreases with the addition of either of the two homopolymers. Correspondingly, the PVPh chains of the block copolymer stretch only slightly for more hydrogen-bonding interfaces with the P4VP chains (cf. the slightly larger D_{mix} in Table 2), whereas these chains remain about the same conformation when associated with PMMA of weak hydrogen bonding affinity, as suggested by a nearly constant layer thickness of the mixed phase (cf. D_{mix} in Table 2).

Upon an increase in the additive volume fraction, a_j/a_{j0} , of the HS/V blend grows continuously for an increasingly larger surface area per chemical junction, leading to interfaces with increasingly higher curvatures that are needed for the successive phases of gyroid, HPC, and BCC spheres (TEM and SAXS results), as elucidated in Figure 10b. With a significantly smaller hydrogen bonding efficiency (cf. Figure 1), the HS/M blend, however, fails to expand a_j large enough for the curvature needed in a lamellar-to-gyroid phase transition (as occurred in the HS/V system). Likely, PMMA homopolymer can only intervene into the PVPh chains at the interface with a limited fraction and then partially phase separates out from the interfacial zone; in terms of the free energy consideration, the modest hydrogen bonding strength between PVPh and PMMA may not be able to compensate, like that of PVPh-P4VP does, the free energy added by the interfaces of increased curvatures for an order-order phase transition.

Interfacial Zone of the Polymer Blends. As mentioned above, the distributions of the three homopolymer additives in the respective polymer blends are characteristically different: the stronger the hydrogen bonding strength is, the higher

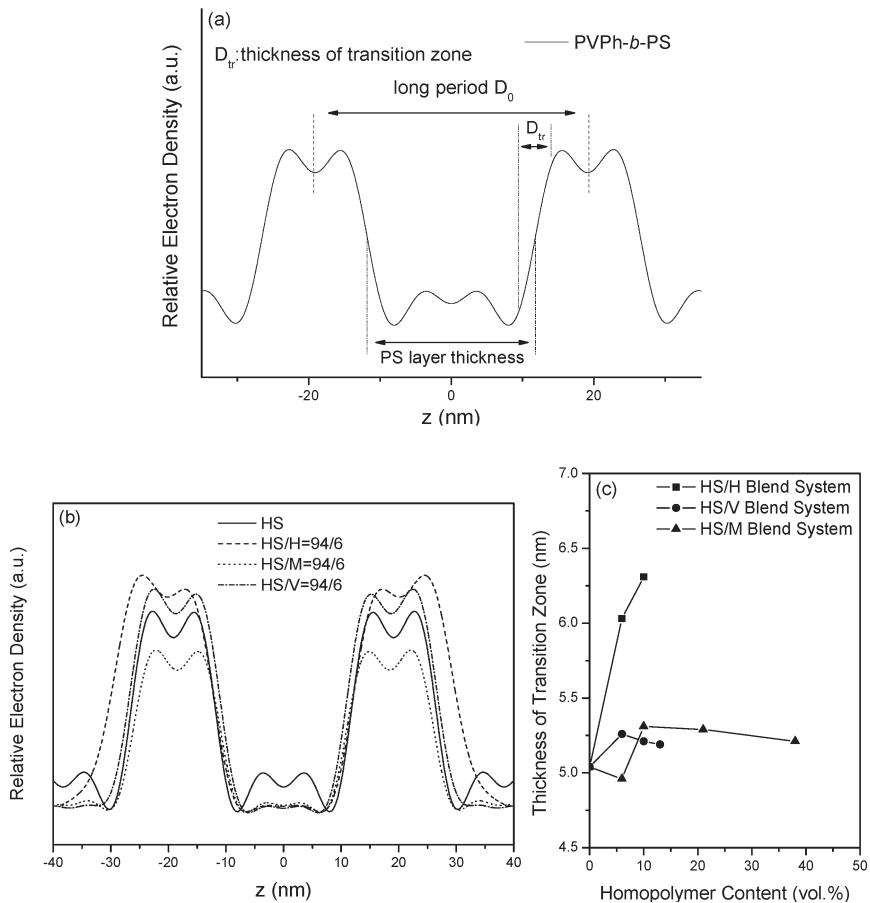


Figure 11. Representative relative electron density profiles of (a) the neat PVPh-*b*-PS and (b) the three blends of HS/H = 94/6, HS/M = 94/6, and HS/V = 94/6. (c) The transition zone thickness D_{tr} extracted for all blends with a lamellar phase at lower volume fractions of homopolymers. In part a, the D_0 and D_{ps} values thus defined are consistent with the values obtained from the 1-D correlation function. The D_{tr} is defined by the zone where the electron density grows from 10 to 90% of the peak value, as illustrated.

the tendency for the additive to stay at the interface. It is interesting to see how the interfacial zone of the respective blends copes with these chain distributions. For this, we have obtained the relative electron density profiles for the blends having a lamellar morphology (Figure 11b) using the direct Fourier transform, as previously described. In general, the respective layer thicknesses of the PS and PVPh-homopolymer phases extracted from the relative electron density profiles of the three types of blends are consistent with those obtained using a 1-D correlation function (Table 2); in addition, the transition zone thickness, D_{tr} , can be defined from the electron density profile, as illustrated in Figure 11a.

Shown in Figure 11c are the D_{tr} values obtained for the three kinds of blends. The obvious increase in D_{tr} from 5.0 to 6.3 nm with the increase in the additive volume fraction up to 10% for the HS/H blends implies significantly disturbed interfaces by the homopolymer. Rather than interdiffusion of PS and PVPh chains at the interface, we attribute the increased D_{tr} to the undulation of lamellar thickness induced by an irregular distribution of the PVPh homopolymer in between the PVPh layers of the copolymer. Consequently, coexistence of swollen and unswollen lamellae can be observed from TEM (cf. Figure 6c) at higher volume fractions of PVPh homopolymer. The D_{tr} changes only marginally (from 5.0 to 5.3 nm) in both the HS/V and HS/M blends in a similar range of homopolymer volume fraction (0–15%); presumably, the added P4VP and PMMA homopolymers selectively reside at the interface areas with the PVPh blocks via hydrogen bonding, and the mixed PVPh

and homopolymer chains act as a collective phase, resulting in a similar transition zone thickness. Because the electron densities of the PVPh, PMMA, and P4VP are all similar, it is difficult to differentiate the distribution of the homopolymer additive of PVPh, PMMA, or P4VP in the PVPh blocks of the copolymer from the SAXS data; small-angle neutron scattering with selected contrast variation will be more direct in addressing the issue of chain conformation of the additive homopolymers in a copolymers–homopolymer blend, as demonstrated by Hashimoto et al.³⁶

Conclusions

We have used FTIR spectroscopy, DSC, TEM, and SAXS techniques to investigate the phase behavior of the HS/V, HS/M, and HS/H blend systems of different hydrogen bonding strengths between the homopolymers and diblock copolymer. Integrated results clearly show that the phase behavior for the A-*b*-B/C type of polymer blends based on PS-*b*-PVPh can be modulated via the hydrogen bonding strength between the homopolymer and copolymer. Fraction of hydrogen bonded groups may be used in quantitatively correlating the hydrogen bonding strength to the phase behavior of the polymer blends. With the interassociation equilibrium constant (K_A) over self-association equilibrium constant (K_B), K_A/K_B , much larger than unity, the phase behavior of the PS-*b*-PVPh/P4VP blend of strong hydrogen bonding strength closely follows that of the neat diblock copolymer; with a K_A/K_B value smaller than unity, the PS-*b*-PVPh/PMMA blend suffers a phase separation, instead of phase transition, at higher homopolymer volume fractions.

Acknowledgment. The work was supported financially by the National Science Council of the ROC under contracts NSC-96-2120-M-009-009 and NSC-96-2218-E-110-008 and Ministry of Education “Aim for the Top University” (MOEATU) program.

Supporting Information Available: Results about FTIR spectroscopic, DSC, and SAXS of diblock copolymer/homopolymer mixtures analyses in this article. This material is available free of charge via the Internet at <http://pubs.acs.org>.

References and Notes

- (1) Muthukumar, M.; Ober, C. K.; Thomas, E. L. *Science* **1997**, *277*, 1225.
- (2) Stupp, S. I.; Braun, P. V. *Science* **1997**, *277*, 1242.
- (3) (a) Hashimoto, T.; Tanaka, H.; Hasegawa, H. *Macromolecules* **1990**, *23*, 4378. (b) Tanaka, T.; Hasegawa, H.; Hashimoto, T. *Macromolecules* **1991**, *24*, 240.
- (4) Moskala, E. J.; Varnell, D. F.; Coleman, M. M. *Polymer* **1985**, *26*, 228.
- (5) Bendejacq, D.; Ponsinet, V.; Joanicot, M. *Macromolecules* **2002**, *35*, 6645.
- (6) Holoubek, J.; Baldrian, J.; Lednický, F.; Malková, S.; Lal, J. *Macromol. Chem. Phys.* **2006**, *207*, 1834.
- (7) Tucker, P. S.; Barlow, J. W.; Paul, D. R. *Macromolecules* **1988**, *21*, 2794.
- (8) Tucker, P. S.; Paul, D. R. *Macromolecules* **1988**, *21*, 2801.
- (9) Lowenhaupt, B.; Steurer, A.; Hellmann, G. P. *Polymer* **1991**, *32*, 1065.
- (10) Lowenhaupt, B.; Steurer, A.; Hellmann, G. P.; Gallot, Y. *Macromolecules* **1994**, *27*, 908.
- (11) Han, Y. K.; Pearce, E. M.; Kwei, T. K. *Macromolecules* **2000**, *33*, 1321.
- (12) Jiang, M.; Xie, H. K. *Prog. Polym. Sci.* **1991**, *16*, 977.
- (13) Jiang, M.; Huang, T.; Xie, J. *Macromol. Chem. Phys.* **1995**, *196*, 787.
- (14) Jiang, M.; Huang, T.; Xie, J. *Macromol. Chem. Phys.* **1995**, *196*, 803.
- (15) Zoelen, W. V.; Ekenstein, G. A. V.; Ikkala, O.; Brinke, G. T. *Macromolecules* **2006**, *39*, 6574.
- (16) Akaba, M.; Nojima, S. *Polym. J.* **2006**, *38*, 559.
- (17) Huang, Y. M.; Liu, H. L.; Hu, Y. *Macromol. Theory Simul.* **2006**, *15*, 321.
- (18) Huang, Y. Y.; Chen, H. L.; Hashimoto, T. *Macromolecules* **2003**, *36*, 764.
- (19) Likhman, A. E.; Semenov, A. N. *Macromolecules* **1997**, *30*, 7273.
- (20) Huang, Y. Y.; Hsu, J. Y.; Chen, H. L.; Hashimoto, T. *Macromolecules* **2007**, *40*, 3700.
- (21) Matsushita, Y. *Macromolecules* **2007**, *40*, 771.
- (22) Stoykovich, M. P.; Edwards, E. W.; Solak, H. H. *Phys. Rev. Lett.* **2006**, *97*, 147802.
- (23) Jinnaí, H.; Hasegawa, H.; Nishikawa, Y.; Sevink, G. J. A.; Braunfeld, M. B.; Agard, D. A.; Spontak, R. J. *Macromol. Rapid Commun.* **2006**, *27*, 1424.
- (24) Lee, J. H.; Balsara, N. P.; Chakraborty, A. K.; Krishnamoorti, R.; Hammouda, B. *Macromolecules* **2002**, *35*, 7748.
- (25) Vaidya, N. Y.; Han, C. D. *Polymer* **2002**, *43*, 3047.
- (26) Huang, P.; Zhu, L.; Cheng, S. Z. D.; Ge, Q.; Quirk, R. P.; Thomas, E. L.; Lotz, B.; Hsiao, B. S.; Liu, L. Z.; Yeh, F. J. *Macromolecules* **2001**, *34*, 6649.
- (27) Vavasour, J. D.; Whitmore, M. D. *Macromolecules* **2001**, *34*, 3471.
- (28) Maurer, W. W.; Bates, F. S.; Lodge, T. P. *J. Chem. Phys.* **1998**, *108*, 2989.
- (29) Jeon, K. J.; Roe, R. J. *Macromolecules* **1994**, *27*, 2439.
- (30) Shull, K. R.; Winey, K. I. *Macromolecules* **1992**, *25*, 2637.
- (31) Bodycomb, J.; Yamaguchi, D.; Hashimoto, T. *Macromolecules* **2000**, *33*, 5187.
- (32) Winey, K. I.; Thomas, E. L.; Fetters, L. J. *Macromolecules* **1992**, *25*, 2645.
- (33) Xie, R.; Li, G.; Liu, C.; Jiang, B. *Macromolecules* **1996**, *29*, 4895.
- (34) Lee, S.-H.; Char, K.; Kim, G. *Macromolecules* **2000**, *33*, 7072.
- (35) Winey, K. I.; Thomas, E. L.; Fetters, L. J. *Macromolecules* **1992**, *25*, 422.
- (36) Koizumi, S.; Hasegawa, H.; Hashimoto, T. *Macromolecules* **1994**, *27*, 7893.
- (37) Yamaguchi, D.; Shiratake, S.; Hashimoto, T. *Macromolecules* **2000**, *33*, 8258.
- (38) Mayes, A. M.; Russell, T. P.; Satija, S. K.; Majkrzak, C. F. *Macromolecules* **1992**, *25*, 6523.
- (39) Kuo, S. W. *Polym. Int.* **2009**, *58*, 455.
- (40) Hameed, N.; Guo, Q. *Polymer* **2008**, *49*, 5268.
- (41) Hameed, N.; Guo, Q. *Macromolecules* **2008**, *41*, 7596.
- (42) Lin, I. H.; Kuo, S. W.; Chang, F. C. *Polymer* **2009**, *50*, 5276.
- (43) Chen, W. C.; Kuo, S. W.; Lu, C. H.; Jeng, U. S.; Chang, F. C. *Macromolecules* **2009**, *42*, 3580.
- (44) Lee, H. F.; Kuo, S. W.; Huang, C. F.; Lu, J. S.; Chan, S. C.; Chang, F. C. *Macromolecules* **2006**, *39*, 5458.
- (45) Kosonen, H.; Ruokolainen, J.; Nyholm, P.; Ikkala, O. *Polymer* **2001**, *42*, 9481.
- (46) Dobrosielska, K.; Wakao, S.; Takano, A.; Matsushita, Y. *Macromolecules* **2008**, *41*, 7695.
- (47) Dobrosielska, K.; Wakao, S.; Suzuki, J.; Noda, K.; Takano, A.; Matsushita, Y. *Macromolecules* **2009**, *42*, 7098.
- (48) Zhao, J. Q.; Pearce, E. M.; Kwei, T. K. *Macromolecules* **1997**, *30*, 7119.
- (49) Chen, W. C.; Kuo, S. W.; Jeng, U. S.; Chang, F. C. *Macromolecules* **2008**, *41*, 1401.
- (50) Lin, C.-L.; Chen, W.-C.; Liao, C. S.; Su, Y.-C.; Huang, C. F.; Kuo, S. W.; Chang, F. C. *Macromolecules* **2005**, *38*, 6435.
- (51) Tung, P. S.; Kuo, S. W.; Chen, S. C.; Lin, C. L.; Chang, F. C. *Polymer* **2007**, *48*, 3192.
- (52) Chen, S. C.; Kuo, S. W.; Liao, C. S.; Chang, F. C. *Macromolecules* **2008**, *41*, 8865.
- (53) Kuo, S. W.; Tung, P. H.; Chang, F. C. *Macromolecules* **2006**, *39*, 9388.
- (54) Lai, Y. H.; Sun, Y. S.; Jeng, U. S.; Lin, J. M.; Lin, T. L.; Sheu, H. S.; Chuang, W. T.; Huang, Y. S.; Hsu, C. H.; Lee, M. T.; Lee, H. Y.; Liang, K. S.; Gabriel, A.; Koch, M. H. J. *J. Appl. Crystallogr.* **2006**, *39*, 871.
- (55) Jeng, U. S.; Su, C. H.; Su, C. J.; Liao, K. F.; Chuang, W. T.; Lai, Y. H.; Chang, J. W.; Chen, Y. J.; Huang, Y. S.; Lee, M. T.; Yu, K. L.; Lin, J. M.; Liu, D. G.; Chang, C. F.; Liu, C. Y.; Chang, C. H.; Liang, K. S. *J. Appl. Crystallogr.*, published online Dec 1, <http://dx.doi.org/10.1107/S0021889809043271>.
- (56) Coleman, M. M.; Graf, J. F.; Painter, P. C. *Specific Interactions and the Miscibility of Polymer Blends*; Technomic Publishing: Lancaster, PA, 1991.
- (57) Moskala, E. J.; Howe, S. E.; Painter, P. C.; Coleman, M. M. *Macromolecules* **1984**, *17*, 1671.
- (58) Chen, H. L.; Wang, S. F.; Lin, T. L. *Macromolecules* **1998**, *31*, 8924.
- (59) Wu, C. M.; Liou, W.; Chen, H. L.; Lin, T. L.; Jeng, U. S. *Macromolecules* **2004**, *37*, 4974.
- (60) Yang, Z.; Han, C. D. *Macromolecules* **2008**, *41*, 2104.
- (61) Kim, E.; Ahn, H.; Ryu, D. Y.; Joo, W.; Kim, J. K.; Jung, J.; Chang, T. *Macromolecules* **2008**, *41*, 9875.